We are IntechOpen, the world's leading publisher of Open Access books Built by scientists, for scientists

4,800
Open access books available

122,000
International authors and editors

135M
Downloads

Our authors are among the

154
Countries delivered to

TOP 1%
most cited scientists

12.2%
Contributors from top 500 universities

WEB OF SCIENCE™

Selection of our books indexed in the Book Citation Index
in Web of Science™ Core Collection (BKCI)

Interested in publishing with us?
Contact book.department@intechopen.com

Numbers displayed above are based on latest data collected.
For more information visit www.intechopen.com

Multi-Objective Control Design with Pole Placement Constraints for Wind Turbine System

Tore Bakka and Hamid Reza Karimi

Additional information is available at the end of the chapter

http://dx.doi.org/10.5772/46403

1. Introduction

The demand for energy world wide is increasing every day. And in these "green times" renewable energy is a hot topic all over the world. Wind energy is currently one of the most popular energy sectors. The growth in the wind power industry has been tremendous over the last decade, its been increasing every year and it is nowadays one of the most promising sources for renewable energy. Since the early 1990s wind power has enjoyed a renewed interest, particularly in the European Union where the annual growth rate is about 20%. It is also a growing interest in offshore wind turbines, either bottom fixed or floating. Offshore wind is higher and less turbulent than the conditions we find onshore. In order to sustain this growth in interest and industry, wind turbine performance must continue to be improved. The wind turbines are getting bigger and bigger which in turn leads to larger torques and loads on critical parts of the structure. This calls for a multi-objective control approach, which means we want to achieve several control objectives at the same time. E.g. maximize the power output while mitigating any unwanted oscillations in critical parts of the wind turbine structure. One of the major reasons the wind turbine is a challenging task to control is due to the nonlinearity in the relationship between turning wind into power. The power extracted from the wind is proportional to the cube of the wind speed.

A wind turbines power production capability is often presented in relation to wind speed, as shown in Fig 1. From the figure we see that the power capability vs. wind speed is divided into four regions of operation. Region I is the start up phase. As the wind accelerates beyond the cut-in speed, we enter region II. A common control strategy in this region is to keep the pitch angle constant while controlling the generator torque. At the point where the wind speed is higher than the rated wind speed of the turbine (rated speed), we enter region III. In this region the torque is kept constant and the controlling parameter is the pitching angle. This is the region we are concerned with in this paper, i.e. the above rated wind speed conditions. The last region is the shutting-down phase (cut-out). The expression for power produced by
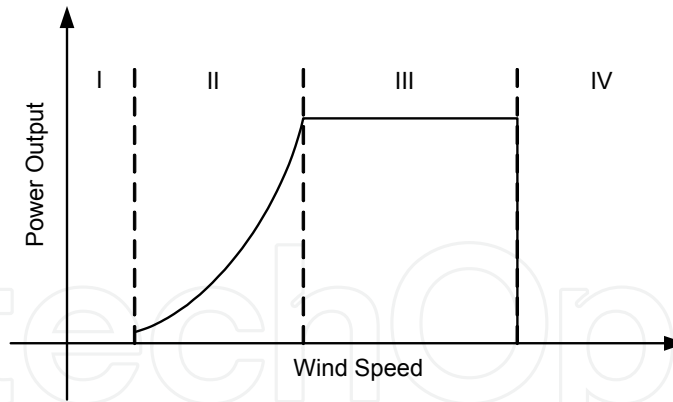
Figure 1. Range of operation for a typical wind turbine

the wind is given by ([1]):

$$P_a = \frac{1}{2}\rho\pi R^2 v^3 C_p(\lambda, \beta) \tag{1}$$

The dimensionless tip-speed ratio (TSR) λ is defined as:

$$\lambda = \frac{v_b}{v} \tag{2}$$

where v_b is the tip speed of the blade and v is the wind speed. From (1) we can find the aerodynamic torque and the thrust force acting on the tower:

$$T_a = \frac{1}{2}\rho\pi R^3 v^2 C_p(\lambda, \beta) \tag{3}$$

$$F_t = \frac{1}{2}\rho\pi R^2 v^2 C_T(\lambda, \beta) \tag{4}$$

where P_a is the aerodynamic power, ρ is the air density, R is the blade radius. C_p gives the relationship between how much power is available in the wind and how much can be converted to electrical power. Not all the available power can be converted, this is due to the fact that the wind can not be completely drained of energy. If it could, the wind speed at the rotor front would reduce to zero and the rotation of the rotor would stop. It can be proven that the theoretical upper limit of C_p is $16/27 \approx 0.59$, which is known as the Betz limit. A typical modern wind turbine has a maximum power coefficient of about 0.5. C_t is the thrust force coefficient, both these coefficients are dependent on the TSR λ and the pitch angle β.

1.1. Modeling and control of wind turbines

1.1.1. Modeling

Whenever we are dealing with control of a wind turbine generating system (WTGS), the turbine becomes a critical part of the discussion. There are many ways to model it, this can be done by simple one mass models ([2]-[3]) or multiple mass models ([4]). Several advanced wind turbine simulation softwares have emerged during the last decade. HAWC2 ([5]), Cp-Lambda ([6]) and FAST ([7]) are a few examples. They are developed at RISØ in Denmark, POLI-Wind in Italy and NREL in the US, respectively. In these codes the turbine and

structure are considered as complex flexible mechanisms, and uses the finite-element-method (FEM) multibody approach. An aero-servo-elastic model is introduced, which consists of aerodynamic forces from the wind, the servo dynamics from the different actuators and the elasticity in the different joints and the structure. Both FAST and HAWC2 can simulate offshore and onshore cases while Cp-Lambda is limited to the onshore case.

1.1.2. Control

Recently, linear controllers have been extensively used for power regulation through the control of blade pitch angle in wind turbine systems e.g. [8]-[15]. However, the performance of these linear controllers are limited by the highly nonlinear characteristics of wind turbines. Advanced control is one research area where such improvement can be achieved.

1.2. Outline of chapter

The paper starts with describing the wind turbine model in section 2. Section 3 deals with control design of the wind turbine system. The system is formulated on a generalized form and the LMI constraints for $\mathcal{H}_2$, $\mathcal{H}_\infty$ and pole placement are developed. Simulation results are presented and evaluated in section 4. Section 5 summarizes the paper and gives the concluding remarks.

2. Wind turbine model

The floating wind turbine model used for the simulation is a 5MW turbine with three blades, which is an upscaled version of Statoils 2.3MW Hywind turbine situated off the Norwegian west coast. The turbine is specified by the National Renewable Energy Laboratory (NREL), more information about the turbine specifications can be found in ([16]). Table 1 shows some of the basic facts of the turbine. The simulation scenario is for above rated wind speed

Rated power	5 $[MW]$
Rated wind speed	11.6 $[m/s]$
Rated rotor speed	12.1 $[RPM]$
Rotor radius	63 $[m]$
Hub hight	90 $[m]$

Table 1. Basic facts of NREL's OC3 turbine

conditions, this means the turbine is operating in region III (see Fig. 1). In this region the major objectives are to maintain the turbines stability, calculate the collective pitch angle in order to prevent large oscillations in the drive train and in the tower and try to keep the rotor and generator at their rated speeds. If we can achieve this, then we keep the power output smooth. The model is obtained from the wind turbine simulation software FAST (Fatigue, Aerodynamics, Structures, and Turbulence). More information about the software can be found in the user's manual ([7]). FAST has two different forms of operation or analysis modes (Fig. 2). The first analysis mode is time-marching of the nonlinear equations of motion - which is, simulation. During simulation, wind turbine aerodynamic and structural response to wind-inflow conditions are determined in time. Outputs of simulation include time-series

data on the aerodynamic loads as well as loads and deflections of the structural parts of the wind turbine. The second form of analysis provided in FAST is linearization. FAST has the capability of extracting linearized representations of the complete nonlinear aeroelastic wind turbine model. Three degrees of freedom are chosen, and they are; rotor, generator and tower
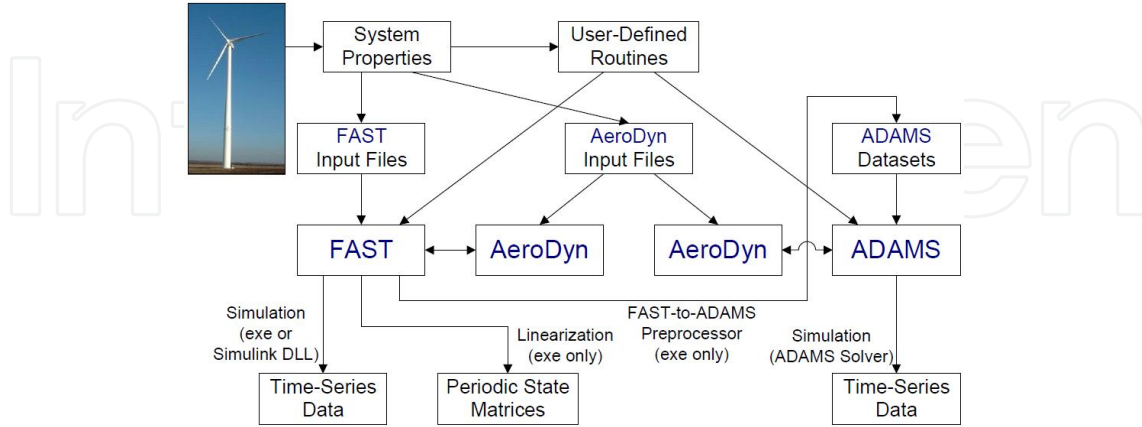

Figure 2. Modes of operation ([7])

dynamics. If desirable, the model can easily be expanded to include more degrees of freedom. The form of the linear model obtained from the software is stated in (5).

$$\dot{x} = \bar{A}x + \bar{B}u$$
$$y = \bar{C}x + \bar{D}u \tag{5}$$

The bar over the matrices in the state space system tells us that these are the average matrices for the wind turbine. FAST calculates the matrices for a state space system at each desired azimuth angle and gives out the average values. The state space system is strictly proper, i.e. $D = 0$. This means that the system will approach zero as the frequency approaches infinity. These average matrices will later be used for the controller design.

The nonlinear model is linearized at a wind speed of 18 $[m/s]$ and at the rated rotors rotational speed 12.1 $[rpm]$. The system has one input and three outputs. Input is pitch angle and the outputs are rotor speed, generator speed and tower fore-aft displacement. The $\bar{A}$ matrix has dimensions 6×6 with the state vector $x = [x_1 \ x_2 \ x_3 \ x_4 \ x_5 \ x_6]^T$, where x_1 is fore-aft displacement, x_2 is generator position, x_3 is rotor position, x_4 is fore-aft speed, x_5 is generator speed and x_6 is rotor speed.

3. Control design

The control purpose of the $\mathcal{H}_\infty$ is to minimize the disturbance effect on the system output. The $\mathcal{H}_2$ purpose is to try to make the system more robust against random disturbances (LQG aspects). With the use of mixed $\mathcal{H}_2/\mathcal{H}_\infty$ control we can benefit from both control synthesis, minimizing possible disturbances effects while rejecting stochastic noise. The control design is solved with the use of linear matrix inequalities (LMIs). These robust control designs mostly

deal with frequency domain aspects of the closed loop system, but it is well known that the location of the closed loop poles play a large role in the transient behavior of the controlled system. In this way we can prevent fast poles and end up with a system which responds in a more realistic way. In the following sections we will use boldface letters to emphasize the LMI optimization variables.

3.1. System representation

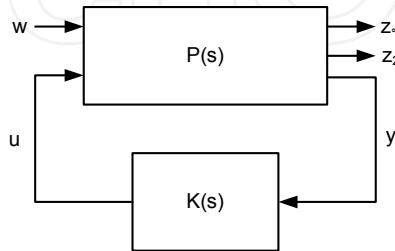Fig. 3 shows the output feedback control scheme. where $P(s)$ is the generalized plant and

Figure 3. Output feedback block diagram

$K(s)$ is the controller. The two blocks represent the equations in (6)-(7). $P(s)$ includes the wind turbine model and the signals of interest

$$
\begin{aligned}
\dot{x} &= Ax + B_1 w + B_2 u \\
z_2 &= C_{21} x + D_1 w + D_2 u \\
z_\infty &= C_{1i} x + D_{1i} w + D_{2i} u \\
y &= C_2 x + D_{21} w + D_{22} u
\end{aligned}
\tag{6}
$$

where A, B_2, C_2 and D_{22} represent the matrices from the standard state space system (5). The other matrices are considered with appropriate dimensions. u is the control input, w is the disturbance signal and y is the measured output. The signals z_2 and z_∞ are, respectively, controlled outputs for $\mathcal{H}_2$ and $\mathcal{H}_\infty$ performance measures. For system (6), the dynamic output feedback $u(s) = K(s)y(s)$, is on the following form:

$$
K(s) \begin{cases} \dot{\zeta} = A_k \zeta + B_k y \\ u = C_k \zeta + D_k y. \end{cases}
\tag{7}
$$

The closed loop system is given in (8) with the states $x_{cl} = [x\ \zeta]^T$.

$$
\begin{aligned}
\dot{x}_{cl} &= A_{cl} x + B_{cl} w \\
z_2 &= C_{cl2} x + D_{cl2} w \\
z_\infty &= C_{cl\infty} x + D_{cl\infty} w
\end{aligned}
\tag{8}
$$

where

$$
\begin{pmatrix}
\begin{array}{c|c}
A_{cl} & B_{cl} \\
\hline
C_{cl2} & D_{cl2} \\
C_{cl\infty} & D_{cl\infty}
\end{array}
\end{pmatrix}
$$

$$= \left(\begin{array}{cc|c} A + B_2 D_k C_2 & B_2 C_k & B_1 + B_2 D_k D_{21} \\ B_k C_2 & A_k & B_k D_{21} \\ \hline C_{21} + D_2 D_k C_2 & D_2 C_k & D_1 + D_2 D_k D_{21} \\ C_{2i} + D_{2i} D_k C_2 & D_{2i} C_k & D_{1i} + D_{2i} D_k D_{21} \end{array} \right). \tag{9}$$

The closed loop transfer functions from w to z_2 and from w to z_∞ are given in (10) and (11) respectively.

$$T_2 = C_{cl2} (sI - A_{cl})^{-1} B_{cl} + D_{cl2} \tag{10}$$

$$T_\infty = C_{cl\infty} (sI - A_{cl})^{-1} B_{cl} + D_{cl\infty} \tag{11}$$

3.2. $\mathcal{H}_2$ Control

The closed loop $\mathcal{H}_2$ norm can be computed as $||T_2||_2^2 = Trace(C_{cl2} \mathbf{S}_0 C_{cl2}^T)$, where $\mathbf{S}_0$ solves the equation

$$A_{cl} \mathbf{S}_0 + \mathbf{S}_0 A_{cl}^T + B_{cl} B_{cl}^T = 0. \tag{12}$$

Since $\mathbf{S}_0 < \mathbf{S}$ for any $\mathbf{S}$ satisfying

$$A_{cl} \mathbf{S} + \mathbf{S} A_{cl}^T + B_{cl} B_{cl}^T < 0 \tag{13}$$

it is verified that $||T_2||_2^2 < \nu$ if and only if there exists $\mathbf{S} > 0$ satisfying (13) and $Trace(C_{cl2} \mathbf{S} C_{cl2}^T) < \nu$. With an auxiliary parameter $\mathbf{Q}$, we obtain the following analysis result; A_{cl} is stable and $||T_2||_2^2 < \nu$ if and only if there exist symmetric $\mathbf{X} = \mathbf{S}^{-1}$ and $\mathbf{Q}$ such that

$$\left(\begin{array}{cc} A_{cl}^T \mathbf{X} + \mathbf{X} A_{cl} & \mathbf{X} B_{cl} \\ * & -I \end{array} \right) < 0$$

$$\left(\begin{array}{cc} \mathbf{X} & C_{cl2}^T \\ * & \mathbf{Q} \end{array} \right) > 0$$

$$trace(Q) < \nu. \tag{14}$$

3.3. $\mathcal{H}_\infty$ Control

The closed loop $\mathcal{H}_\infty$ norm is defined in (15).

$$||T_{cl}||_\infty < \gamma \tag{15}$$

In order to formulate the $\mathcal{H}_\infty$ norm in terms of a matrix inequality, we need to do some manipulations to its original expression. It is known that the ∞-norm of a closed loop system is the same as taking the 2-norm of the signals of interest z divided by the 2-norm of the systems exogenous input w. In this way we will end up with the famous Bounded Real Lemma (BRL). First, lets define Lyapunovs stability criteria. A linear state space system (8) is asymptotically stable if all real parts of the eigenvalues of the A_{cl}-matrix are negative. The Lyapunov criteria involves searching for the matrix $\mathbf{X}$, if it exists then the system is stable. A quadratic Lyapunov function is defined in (16) and its derivative in (17).

$$V(x) = x^T \mathbf{X} x \tag{16}$$

$$\dot{V}(x) = \dot{x}^T \mathbf{X} x + x^T \mathbf{X} \dot{x} \tag{17}$$

The first crucial steps in obtaining the BRL are shown next. Firstly we remove the roots by squaring both sides of the inequality sign. Secondly we collect everything in one integral expression and lastly we do the trick where we add and subtract the Lyapunov function to the inequality. We can do this because we know that $\int_0^\infty \dot{V}(x) - V(\infty) + V(0) = 0$ is true. By doing this we only end up with the integral expression.

$$\frac{||z||_2}{||w||_2} < \gamma \;\Rightarrow\; \left[\int_0^\infty z^T z \, dt\right]^{\frac{1}{2}} < \gamma \left[\int_0^\infty w^T w \, dt\right]^{\frac{1}{2}}$$

$$\Rightarrow \int_0^\infty \left(\frac{1}{\gamma} z^T z - \gamma w^T w + \dot{V}(x)\right) dt + \underbrace{V(0)}_{\text{Always zero}} \quad \underbrace{-V(\infty)}_{\text{Always negative}} < 0 \qquad (18)$$

Now we insert both the expression for the signal of interest z from (8) and the derivative of the Lyapunov function $\dot{V}(x)$ (17) into (18). We do some algebraic and matrix manipulations and end up with the following matrix inequality (BRL). This is not yet an LMI because of the nonlinear terms which occur when the feedback loop is closed.

$$\begin{pmatrix} A_{cl}^T \mathbf{X} + \mathbf{X} A_{cl} & \mathbf{X} B_{cl} & C_{cl\infty}^T \\ * & -\gamma I & D_{cl\infty}^T \\ * & * & -\gamma I \end{pmatrix} < 0$$

$$\mathbf{X} > 0 \qquad (19)$$

3.4. Change of variables

For the multi-objective case we want to create a feedback controller $u = K(s)y$ through minimization of the trade off criterion in (20)

$$J = \alpha ||T_\infty||_\infty^2 + \beta ||T_2||_2^2 \qquad (20)$$

where α and β are the weights. As mentioned, the $\mathcal{H}_2$ and $\mathcal{H}_\infty$ constraints (14) and (19) are not yet LMIs. In order to transform these nonlinear terms into proper LMIs we linearize them with the use of change of variables. This is not as straight forward as for the state feedback case, where $\mathbf{X} = \mathcal{P}^{-1}$ and $\mathbf{F} = F\mathcal{P}^{-1}$ turn all constraints into LMIs. More details about the change of variables can be found in ([17])

The new matrices $\mathcal{P}$ and $\mathcal{P}^{-1}$ are partitioned as follows,

$$\mathcal{P} = \begin{bmatrix} \mathbf{X} & N \\ N^T & \# \end{bmatrix}, \qquad \mathcal{P}^{-1} = \begin{bmatrix} \mathbf{Y} & M \\ M^T & \# \end{bmatrix} \qquad (21)$$

where $\mathbf{X}$ and $\mathbf{Y}$ are symmetric matrices of dimension $n \times n$. N and M will be calculated on the basis of $\mathbf{X}$ and $\mathbf{Y}$ at the end of this section. The matrices noted as # are not necessary to be

known. In addition, we define the following two matrices,

$$\Pi_1 = \begin{bmatrix} \mathbf{Y} & I \\ M^T & 0 \end{bmatrix}, \qquad \Pi_2 = \begin{bmatrix} I & \mathbf{X} \\ 0 & N^T \end{bmatrix} \tag{22}$$

as can be inferred from the identity $\mathcal{P}\mathcal{P}^{-1} = I$ satisfying

$$\mathcal{P}\Pi_1 = \Pi_2. \tag{23}$$

Now we are ready to convert the nonlinear matrix inequalities into LMIs. This is done by performing congruence transformation with $diag(\Pi_1, I, I)$ and $diag(\Pi_1, I)$ on the $\mathcal{H}_\infty$ and $\mathcal{H}_2$ constraints respectively. We now obtain the following LMIs

$$\begin{pmatrix} sym\left(A\mathbf{X} + B_2\hat{\mathbf{C}}\right) & \hat{\mathbf{A}}^T + A + B_2\hat{\mathbf{D}}C_2 & B_1 + B_2\hat{\mathbf{D}}D_{21} & \mathbf{X}C_{1i}^T + \hat{\mathbf{C}}^T D_{21}^T \\ * & sym\left(\mathbf{Y}A + \hat{\mathbf{B}}C_2\right) & \mathbf{Y}B_1 + \hat{\mathbf{B}}D_{21} & C_{1i}^T + C_2^T\hat{\mathbf{D}}^T + D_{2i}^T \\ * & * & -\gamma I & D_{1i}^T + D_{21}^T\hat{\mathbf{D}}D_{2i}^T \\ * & * & * & -\gamma I \end{pmatrix} < 0$$

$$\begin{pmatrix} sym\left(A\mathbf{X} + B_2\hat{\mathbf{C}}\right) & \hat{\mathbf{A}}^T + A + B_2\hat{\mathbf{D}}C_2 & B_1 + B_2\hat{\mathbf{D}}D_{21} \\ * & sym\left(\mathbf{Y}A + \hat{\mathbf{B}}C_2\right) & \mathbf{Y}B_1 + \hat{\mathbf{B}}D_{21} \\ * & * & -I \end{pmatrix} < 0$$

$$\begin{pmatrix} \mathbf{X} & I & \left(C_{12}\mathbf{X} + D_2\hat{\mathbf{C}}\right)^T \\ * & \mathbf{Y} & \left(C_{12} + D_2\hat{\mathbf{D}}C_2\right)^T \\ * & * & \mathbf{Q} \end{pmatrix} > 0$$

$$trace(\mathbf{Q}) < \nu_0$$

$$\gamma < \gamma_0 \tag{24}$$

where $sym(A)$ is defined as $A + A^T$. Now following identities can be obtained

$$\Pi_1^T \mathcal{P}\mathcal{A}\Pi_1 = \Pi_2^T \mathcal{A}\Pi_1 = \begin{bmatrix} A\mathbf{X} + B_2\hat{\mathbf{C}} & A + B_2\hat{\mathbf{D}}C_2 \\ \hat{\mathbf{A}} & \mathbf{Y}A + \hat{\mathbf{B}}C_2 \end{bmatrix} \tag{25}$$

$$\Pi_1^T \mathcal{P}\mathcal{B} = \Pi_2^T \mathcal{B} = \begin{bmatrix} B_1 + B_2\hat{\mathbf{D}}D_{21} \\ \mathbf{Y}B_1 \end{bmatrix} \tag{26}$$

$$\mathcal{C}\Pi_1 = \begin{bmatrix} C_{1i}\mathbf{X} + D_{21}\hat{\mathbf{C}} & C_{1i} + D_{21}\hat{\mathbf{D}} \end{bmatrix} \tag{27}$$

$$\Pi_1^T \mathcal{P}\Pi_1 = \Pi_1^T \Pi_2 = \begin{pmatrix} \mathbf{X} & I \\ I & \mathbf{Y} \end{pmatrix}. \tag{28}$$

In order for (28) to be true the following relationship must hold

$$MN^T = I - \mathbf{XY}. \tag{29}$$

This relationship can be solved by utilizing the singular value decomposition (SVD). We know that s_d is a diagonal matrix and we define a new matrix $\bar{s}_d$, which is the square root of all the entries in s_d. In this way we can find the matrices M and N as shown below.

$$svd(I - \mathbf{XY}) = us_d v^T \tag{30}$$

$$\bar{s}_d = diag(sqrt(s_d)) \tag{31}$$

$$M = u\bar{s}_d \tag{32}$$

$$N^T = \bar{s}_d v^T \tag{33}$$

3.5. LMI region

An LMI region is any convex subset D of the complex plane that can be characterized as an LMI in z and $\bar{z}$ ([18])

$$D = \{z \in C : L + \bar{M}z + \bar{M}^T\bar{z} < 0\} \tag{34}$$

for fixed real matrices $\bar{M}$ and $L = L^T$, where $\bar{z}$ is a complex number. This class of regions encompasses half planes, strips, conic sectors, disks, ellipses and any intersection of the above. From ([18]), we find that all eigenvalues of the matrix A is in the LMI region $\{z \in C : [l_{ij} + \bar{m}_{ij}z + \bar{m}_{ji}\bar{z}]_{i,j} < 0\}$ if and only if there exists a symmetric matrix $\mathbf{X}_D$ such that

$$\left[l_{ij}\mathbf{X}_D + \bar{m}_{ij}A^T\mathbf{X}_D + \bar{m}_{ji}\mathbf{X}_DA\right]_{i,j} < 0, \quad \mathbf{X}_D > 0. \tag{35}$$

Also, here we need to include the change of variables. This is done in (36) where $\otimes$ denotes the Kronecker product.

$$\left(L \otimes \begin{pmatrix} \mathbf{X} & I \\ I & \mathbf{Y} \end{pmatrix} + \bar{M} \otimes \begin{pmatrix} A\mathbf{X} + B\hat{\mathbf{C}} & A + B\hat{\mathbf{D}}C \\ \hat{\mathbf{A}} & \mathbf{Y}A + \hat{\mathbf{B}}C \end{pmatrix}\right.$$
$$\left. + \bar{M}^T \otimes \begin{pmatrix} A\mathbf{X} + B\hat{\mathbf{C}} & A + B\hat{\mathbf{D}}C \\ \hat{\mathbf{A}} & \mathbf{Y}A + \hat{\mathbf{B}}C \end{pmatrix}^T\right) < 0 \tag{36}$$

As an example we define the desired region D as a disk (Fig. 4), with center located along the x-axis (distance q from the origin) and radius r. This determines the region

$$D = \begin{pmatrix} -r & q+z \\ q+\bar{z} & -r \end{pmatrix} \tag{37}$$

where the closed loop eigenvalues may be placed.

From this we can find that the matrices L and $\bar{M}$ have the following form

$$L = \begin{pmatrix} -r & q \\ q & -r \end{pmatrix}, \qquad \bar{M} = \begin{pmatrix} 0 & 1 \\ 0 & 0 \end{pmatrix}. \tag{38}$$

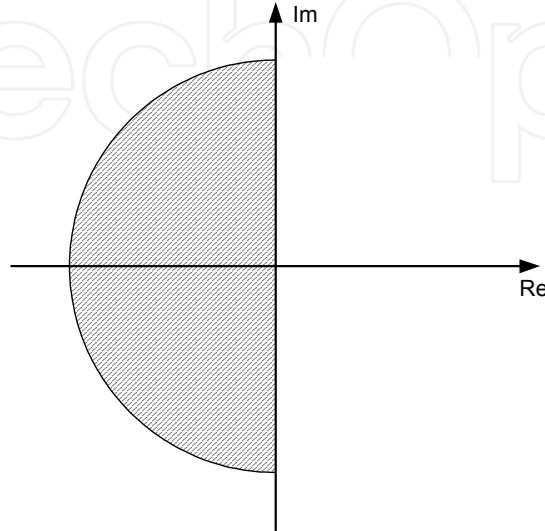All the constraints in (24) and the constraint in (36) are subjected to the minimization of the

Figure 4. LMI region

objective function given in (20). They need to be solved in terms of $\left(\mathbf{X}, \mathbf{Y}, \mathbf{Q}, \hat{\mathbf{A}}, \hat{\mathbf{B}}, \hat{\mathbf{C}}, \hat{\mathbf{D}} \right)$.

Finally, the controller matrices can be found by the following relationship

$$D_k = \hat{\mathbf{D}} \tag{39}$$

$$C_k = \left(\hat{\mathbf{C}} - D_k C_2 \mathbf{X} \right) \left(M^T \right)^{-1} \tag{40}$$

$$B_k = N^{-1} \left(\hat{\mathbf{B}} - \mathbf{Y} B_2 D_k \right) \tag{41}$$

$$A_k = N^{-1} \left(\hat{\mathbf{A}} - N B_k C_2 \mathbf{X} - \mathbf{Y} B_2 C_k M^T - \mathbf{Y} \left(A + B D_k C_2 \right) \mathbf{X} \right) \left(M^T \right)^{-1}. \tag{42}$$

From the aforementioned expressions we are able to solve the mixed H_2/H_∞ control problem with pole placement constraints.

4. Simulation

All calculations and simulations are carried out in MatLab/Simulink ([19]) interfaced with YALMIP ([20]). The solver which is used for the LMI calculation is SeDuMi ([21]). FAST comes with a Simulink template which can be changed how ever the user may see fit. As described earlier the simulation scenario is for the above rated wind speed situation. We want to mitigate oscillations in the drive train and dampen tower movement while maintaining the rotors rated rotational speed. Satisfactory simulation results were found with $\alpha = 1$ and $\beta = 1$

as weights for the objective function and with the following performance measures:

$$z_2 = x_4 + x_5 - x_6 + u \tag{43}$$

$$z_\infty = x_1 + x_2 - x_3. \tag{44}$$

The norms obtained from the optimization are shown in (45) and the closed loop poles are shown in Fig. (5).

$$trace(\mathbf{Q}) = 9.995 \quad \gamma = 27.7216 \tag{45}$$

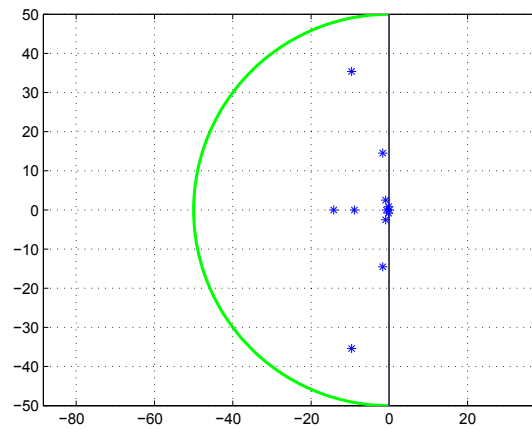In order to find the performance measures we argue that there are no oscillations in the drive
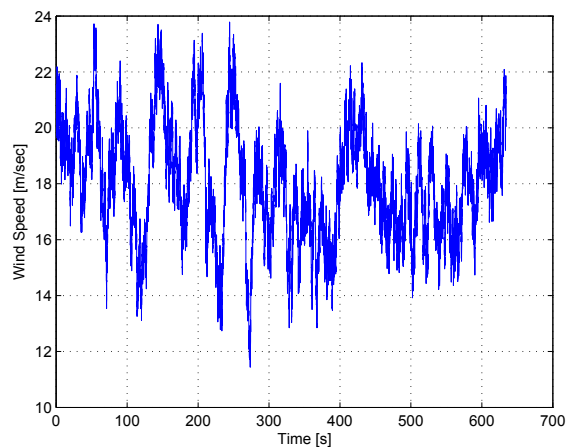

Figure 5. Closed loop poles

Figure 6. Wind profile

train if the position of the generator and the rotor are the same. In other words we must try to keep $x_2 - x_3$ close to zero. Similar procedure is done for the speed difference and the tower's speed and position. The wind profile is obtained from the software TurbSim ([22]), which is also developed at the NREL. This is a stochastic, full-field, turbulent-wind simulator, and the output can be used as input to FAST. The profile is a 50 year extreme wind condition, with an average speed of 18 $[m/s]$ and a turbulence intensity of 17 %. The waves have a significant wave hight of 6 $[m]$ and a peak wave period of 10 $[s]$.

As a consequence of having better performance the pitching activity has heavily increased, see Fig. 10. The pitching activity lies around $5 - 10 \, [deg/s]$, which is within the limits of a modern wind turbine. The output torque is presented in Fig. 11, which also shows better performance.
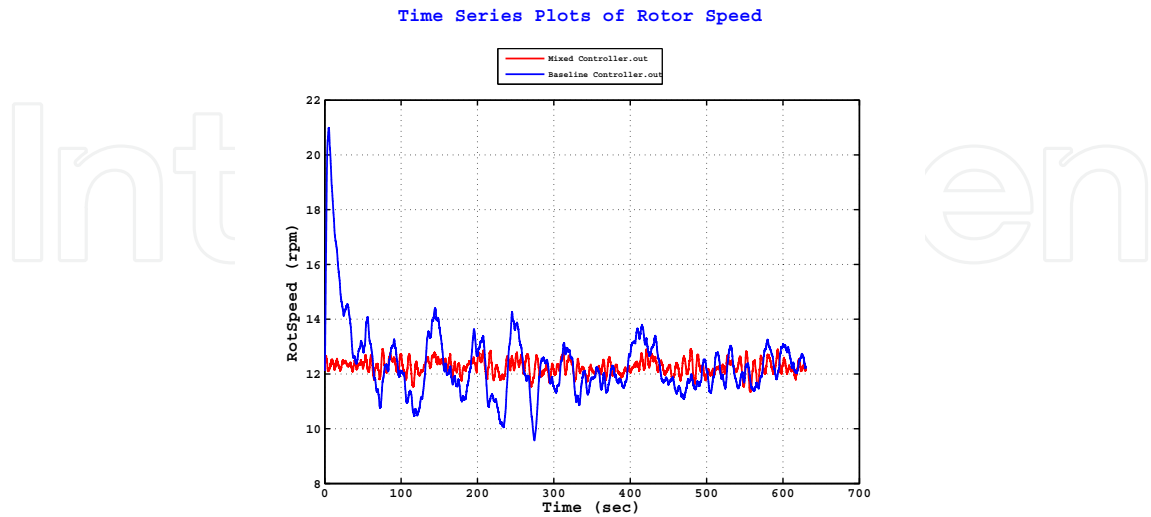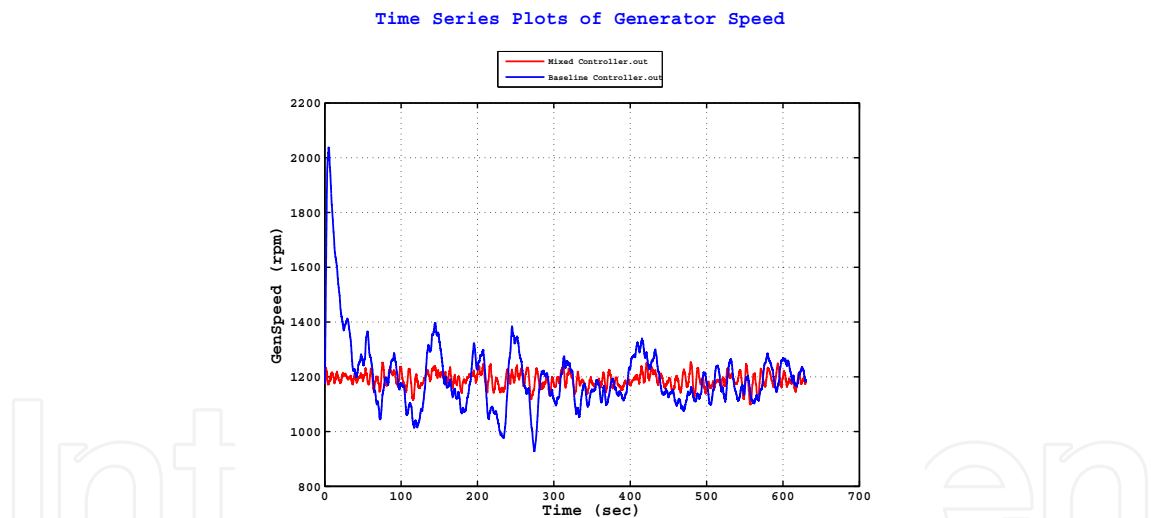

Figure 7. Rotor speed

Figure 8. Generator speed

The controller is tested on the fully nonlinear system, where the only degrees of freedom which are left out are yaw and translational surge. The state space system of the controller is shown in the appendix. The plots included in this chapter are the same ones that were used as feedback to the controller. That is, rotor rotational speed (Fig. 7), generator rotational speed (Fig. 8) and tower fore-aft displacement (Fig. 9). The simulation results show a comparison between our simulations and simulations done with FAST's baseline controller. The baseline controller is a gain scheduled PI controller and is indicated on the plots as the blue line. The controller proposed in this chapter is indicated with the red line.
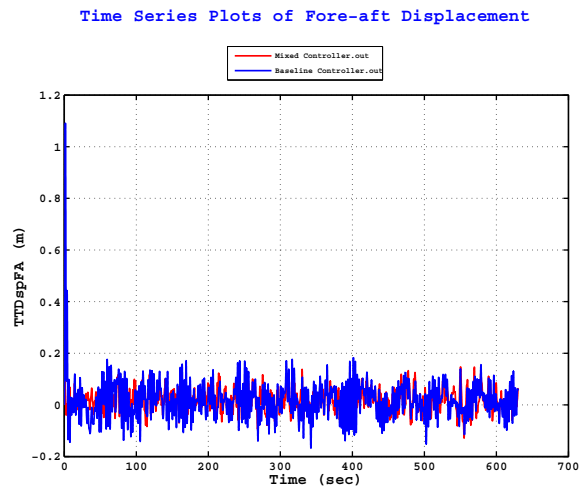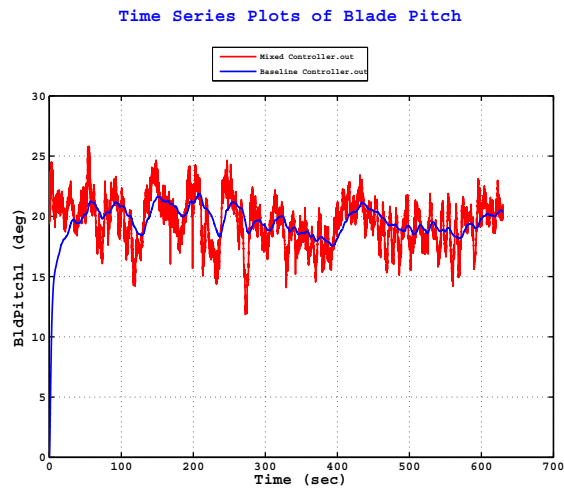
Figure 9. Tower fore-aft displacement

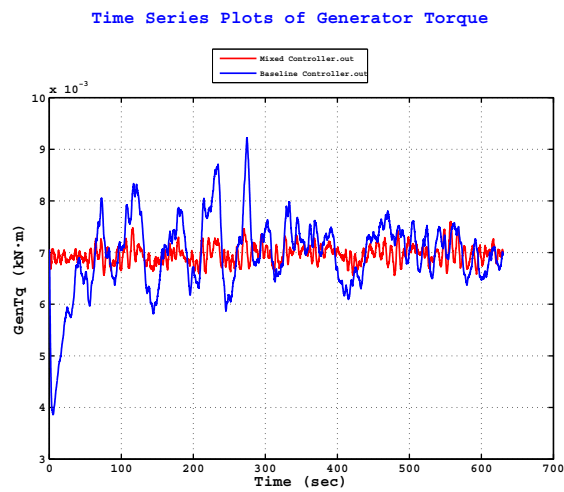**Figure 10.** Blade pitch angle

Figure 11. Generator output torque

5. Conclusion

In this chapter we have introduced a nonlinear model of an offshore floating wind turbine using the commercial wind turbine software FAST. By the use of its embedded routines a linear model is extracted. The linear model used in this chapter is built up with relatively few degrees of freedom. More degrees of freedom can easily be added to the model, depending on the control objectives. In our approach this relatively simple model serves its purpose in testing advanced control routines on an offshore floating wind turbine system. On the basis of this linear model a mixed $\mathcal{H}_2/\mathcal{H}_\infty$ control with pole placement constraint is designed, tested and compared with FAST's baseline controller. The proposed controller is tested on the nonlinear wind turbine model under the influence of a 50 year extreme wind condition, 6 $[m]$ significant wave hight and 10 $[s]$ peak wave period. The control objectives have been to mitigate unwanted oscillations in the drive train and tower, in addition to maintain the rotor and generator rotational speeds at their rated values. If any unwanted oscillations in the drive train are damped and rated speed is maintained, the torque output should be smooth. Our proposed control shows better performance than FAST's baseline controller.

Acknowledgment

Author details

Tore Bakka and Hamid Reza Karimi
University of Agder, Norway

Appendix

State space system of wind turbine model:

$$\dot{x} = \begin{bmatrix} 0 & 0 & 0 & 1 & 0 & 0 \\ 0 & 0 & 0 & 0 & 1 & 0 \\ 0 & 0 & 0 & 0 & 0 & 1 \\ -5.4263 & -1.7533\times10^{-5} & -1.8036\times10^{-5} & -0.29188 & -2.3801 & -2.3801 \\ 0 & 0 & 172.6 & 0 & 12.082\times10^{-5} & 1.237 \\ -1.0727\times10^{-3} & 6.6008\times10^{-7} & -195 & -0.027639 & -0.37886 & -1.7757 \end{bmatrix} x + \begin{bmatrix} 0 \\ 0 \\ 0 \\ -9.913 \\ 0 \\ -1.5151 \end{bmatrix} u$$

$$y = \begin{bmatrix} 0 & 0 & 0 & 0 & 9.549 & 9.549 \\ 0 & 0 & 0 & 0 & 926.3 & 0 \\ 1 & 0 & 0 & 0 & 0 & 0 \end{bmatrix} x + \begin{bmatrix} 0 \\ 0 \\ 0 \end{bmatrix} u \tag{46}$$

State space system of the controller:

$$\dot{\zeta} = \begin{bmatrix} -26.6610 & -30.6408 & 0.8454 & -0.1632 & 0.6128 & -0.0186 \\ 101.0655 & 81.5111 & 0.8504 & 0.9437 & -2.5035 & 0.0951 \\ -196.7809 & -173.8849 & -1.1085 & -3.2463 & 6.4727 & -0.1600 \\ 42.9129 & 52.3436 & -0.1755 & -3.0062 & -0.2203 & 0.1970 \\ 1239.7 & 1063.4 & 11.6 & 20.4 & -39.6 & 1.1 \\ -47346.0 & -43037.0 & -91.0 & -306.0 & 1178.0 & -55.0 \end{bmatrix} \zeta$$

$$+ \begin{bmatrix} -0.5521 & -0.0185 & -12.2055 \\ -3.5502 & 0.0763 & 14.6491 \\ 12.5597 & -0.1696 & 0.2177 \\ 6.6856 & 0.0668 & -25.7465 \\ -95.4987 & 1.0100 & 6.3680 \\ 1988.8 & -44.3 & -2523.0 \end{bmatrix} u$$

$$u = \begin{bmatrix} 0.2036 & 1.3748 & -0.1657 & 0.0032 & -0.0026 & -0.0008 \end{bmatrix} \zeta$$

$$+ \begin{bmatrix} 0.2132 & -0.0001 & 1.3252 \end{bmatrix} u \tag{47}$$

6. References

[1] D. M. Eggleston and F. S. Stoddard. *Wind Turbine Engineering Design*. Van Nostrand Reinhold Co., New York, 1987.

[2] J. Tamura, T. Yamajaki, M. Ueno, Y. Matsumura, and S. Kimoto. Transient stability simulation of power system including wind generator by PSCAD/EMTDC. In *IEEE Porto Power Tech Conference*, September 2001.

[3] E. S. Abdin and W. Xu. Control design and dynamic performance analysis of a wind turbine induction generator unit. *IEEE Transactions on Energy Conversion*, Vol. 15(No. 1):91–96, March 2000.

[4] R. Takahashi T. Murata J. Tamura Y. Tomaki A. Sakahara S.M. Muyeen, Md. Hasan Ali and E. Sasano. Comparative study on transient stability analysis of wind turbine generator system using different drive train models. *IET Renewable Power Generation*, Vol. 1(No. 2):131 – 141, June 2007.

[5] T. J. Larsen. How 2 HAWC2, the user's manual. In *Risø-R-1597(ver. 3-9)(EN)*, September 2009.

[6] C.L. Bottasso and A. Croce. Cp-Lambda user manual. In *RisÃÿ-R-1597(ver. 3-9)(EN)*. Dipartimento di Ingnegneria Aerospaziale, Politecnico di Milano, September 2009.

[7] J. Jonkman and M. L. Buhl. FAST User's Guide. In *Technical Report NREL/EL-500-38230*, September 2009.

[8] R. Eide and H. R. Karimi. *Control Design Methodologies for Vibration Mitigation on Wind Turbine Systems*. InTech, Vibration Analysis and Control - New Trends and Developments, Dr. Francisco Beltran-Carbajal (Ed.), pp. 217-242, ISBN: 978-953-307-433-7, 2011.

[9] H.R. Karimi. Wavelet-based optimal control of a wind turbine system: A computational approach. *J. Advanced Mechanical Design, Systems and Manufacturing*, Vol. 5(No. 3):171–186, 2011.

[10] B. Skaare, T. D. Hanson, and F. G. Nielsen. Importance of control strategies on fatigue life of floating wind turbines. In *Proceedings of 26th International Conference on Offshore Mechanics and Arctic Engineering*, pages 493–500, June 2007.

[11] J. Jonkman. Influence of control on the pitch damping of a floating wind turbine. In *ASME Wind Energy Symposium*, 2008.

[12] H. Namik and K. Stol. Individual blade pitch control of floating offshore wind turbines. *Wind Energy*, Vol. 13(No. 1):74 – 85, 2009.

[13] S. Christiansen, T. Knudsen, and T. Bak. Optimal control of a ballast- stabilized floating wind turbine. In *IEEE Multi-Conference on Systems and Control*, pages 1214 – 1219, Colorado, Denver, September 2011.

[14] E. Wayman, P. Sclavounos, S. Butterfield, J. Jonkman, and W. Musial. Coupled dynamic modeling of floating wind turbine systems. In *Offshore Technology Conference*, Houston, Texas, May 2006.

[15] T. D. Hanson, B. Skaare, R. Yttervik, F. G. Nielsen, and O. HavmÃ¿ller. Comparison of measured and simulated responses at the first full scale floating wind turbine hywind. In *EWEA*, Brussels, February 2011.

[16] J. Jonkman, S. Butterfield, W. Musial, and G. Scott. Definition of a 5-MW reference wind turbine for offshore system development. In *Technical Report NREL/TP-500-38060*. National Renewable Energy Laboratory, February 2009.

[17] C. Scherer, P. Gahinet, and M. Chilali. Multiobjective outputfeedback control via LMI optimization. *IEEE Transactions on Automatic Control*, Vol. 42(No. 7):896 – 911, July 1997.

[18] M. Chilali and P. Gahinet. h_∞ design with pole placement constraints: An LMI approach. *IEEE Transactions on Automatic Control*, Vol. 41(No. 3):358 – 367, March 1996.

[19] MATLAB. *version 7.10.0 (R2010a)*. The MathWorks Inc., Natick, Massachusetts, 2010.

[20] Johan Löfberg. Yalmip : a toolbox for modeling and optimization in MATLAB. In *2004 IEEE International Symposium on Computer Aided Control Systems Design*, pages 284 – 289, Taipei, Taiwan, February 2005.

[21] J. F. Strum. Using SeDuMi 1.02, a MatLab toolbox for optimization over symmetric cones. In *Optimization Methods and Software*, pages 625 – 653, 1999.

[22] B. J. Jonkman. TurmSim user'guide: Version 1.50. In *Technical Report NREL/EL-500-46198*. National Renewable Energy Laboratory, September 2009.